Organic Electronics 13 (2012) 652–666

Contents lists available at SciVerse ScienceDirect

Organic Electronics

journal homepage: www.elsevier.com/locate/orgel

Efficient bulk heterojunction photovoltaic devices based on diketopyrrolopyrrole containing small molecule as donor and modified PCBM derivatives as electron acceptors

G.D. Sharma [a,b,*], J.A. Mikroyannidis [c], S.S. Sharma [d], M.S. Roy [f], K.R. Justin Thomas [e,*]

[a] Physics Department, Molecular Electronic and Optoelectronic Device Laboratory, JNV University, Jodhpur, Rajasthan 342005, India
[b] R&D Center for Science and Engineering, Jaipur Engineering College, Kukas, Jaipur, Rajasthan, India
[c] Chemical Technology Laboratory, Department of Chemistry, University of Patras, GR-26500 Patras, Greece
[d] Department of Engineering Physics, Govt. Engineering College for Women, Ajmer, Rajasthan, India
[e] Organic Materials Lab, Department of Chemistry, Indian Institute of Technology, Roorkee, Uttrakhand, India
[f] Defence Laboratory, Jodhpur, Rajasthan, India

ARTICLE INFO

Article history:
Received 26 July 2011
Received in revised form 13 November 2011
Accepted 19 November 2011
Available online 16 January 2012

Keywords:
Diketopyrrolopyrrole small molecule
Modified PCBM
Bulk heterojunction
Photovoltaic devices

ABSTRACT

A new solution processable small molecule (DPP–CN) containing electron donor diketopyrrolopyrrole (DPP) core and cyanovinylene 4-nitrophenyl (CN) electron acceptor has synthesized for use as the donor material in the bulk heterojunction organic solar cells along with PCBM, modified PCBM i.e. F and A as electron acceptor. It showed a broad absorption in longer wavelength region having optical band gap around 1.64 eV. We have used PCBM, F and A as electron acceptor for the fabrication of bulk heterojunction photovoltaic devices. The power conversion efficiency (PCE) of the BHJ devices based on DPP–CN:PCBM, DPP–CN:F and DPP–CN:A blends cast from the THF solvent is 1.83%, 2.79% and 2.83%, respectively. The increase in the PCE based on F and A as electron acceptor is mainly due to the increase in both short circuit current (J_{sc}) and open circuit voltage (V_{oc}). The PCE value of the photovoltaic devices based on the blends DPP–CN:PCBM, DPP–CN:F and DDP–CN:A cast from the mixed solvents (DIO/THF) has been further improved up to 2.40%, 3.32% and 3.34%, respectively. This improvement is mainly due to the increased value of J_{sc}, which is attributed not only to the increase of crystallinity, but also to the morphological change in the film cast from mixed solvent. Finally, the device ITO/PEDOT:PSS/DPP–CN:A (DIO/THF cast)/TiO_2/Al device shows a PCE of 3.9%. The improved device performance could be attributed to the electron transporting and hole-blocking capabilities due to the introduced TiO_2 buffer layer.

1. Introduction

Organic photovoltaic (OPV) cells based on bulk heterojunction (BHJ) materials compromising of a π-conjugated (semiconducting) polymers and fullerene derivatives have offered special opportunities due to the their promising photovoltaic performance and facile fabrication by means of low cost solution processing techniques and makes them effective alternative to the silicon based solar cells [1,2]. The active layer in the BHJ OPVs is the admixture of organic donor and acceptor. The organic donor and acceptor materials used in the BHJ active layer strongly affect the photovoltaic performance of OPVs. The Power conversion efficiency (PCE) of devices based on organic semiconducting materials are predicted to reach 15% by modeling [3]. The current effort in this community was focused on developing low band gap polymers to harvest the photons from the longer wavelength regions. During last two years, several low band gap polymers with enhanced

* Corresponding authors. Address: Physics Department, Molecular Electronic and Optoelectronic Device Laboratory, JNV University, Jodhpur, Rajasthan 342005, India (G.D. Sharma).
E-mail address: sharmagd_in@yahoo.com (G.D. Sharma).

1566-1199/$ - see front matter © 2011 Elsevier B.V. All rights reserved.
doi:10.1016/j.orgel.2011.11.021

absorption abilities were developed and researchers made a breakthrough in fabricating OPV devices with PCEs up to 5–7.5% based on these polymers [4]. To date, the PCEs based on conjugated polymers have reached high up to 8.13%, reported by Solarmer [5a]. A PCE of 8.3% has been recently reported by Konarka, for OPV, which is a current world record [5b]. It can be seen that there is still a gap between the practical efficiency and the theoretical one. Therefore, it is critically important to design and synthesis new donor or acceptor materials for achieving higher PCE.

Generally, organic polymers posses the advantages of strong absorption ability, admirable solution processability, good film forming ability and tunable highest occupied molecular orbital (HOMO) and lowest unoccupied molecular orbital (LUMO) energy levels. However, the purification of polymers is one of the most difficult problems. For example, it is very difficult to separate the Pd-catalyst from the polymer [6]. As usual, a polymer is a mixture of molecules with different molecular weights. The impurity and relatively high dispersity of molecular weight would significantly decrease the charge carrier mobility of polymers and further lead to relative fill factor (FF) and PCE in the resulting photovoltaic devices [7]. In contrast to polymers, small molecules semiconductors for BHJ organic solar cells are attractive because of their advantages over their counterparts, which include well defined molecular structure, definite molecular weight, and high purity without batch to batch variations [8]. In recent years, a great amount of effort has been dedicated to develop new solution processable small molecules and corresponding photovoltaic devices [9,10]. The best PCE of BHJ solar cells based on the solution processable small molecules has been reported by Nguyen and co-workers, which is about 3.0–4.4% [11]. Recently, Chen and co-workers [11e] have reported a PCE of 5.06% based on a BHJ active layer of the thiophene small molecules end-capped with electron withdrawing alkyl cyanoacetate groups as electron donor and PCBM as electron acceptor. The mismatch between the absorption spectrum of small molecules and the solar spectrum is still one of the primary problems for improving the PCE of photovoltaic devices. Therefore more attention is being directed to design and synthesis of small molecules with donor–acceptor (D–A) structure [12]. The intramolecular charge transfer (ICT) from the donor moiety to the acceptor moiety inside the D–A molecules can efficiently extend the absorption spectrum of the molecule for better matching with the solar spectrum. Moreover, the incorporation of electron withdrawing moiety with different electron donating moieties will bring different ICT degrees to the conjugated molecules and thus provide a means to tune their energy levels [13]. Therefore, from the point of view, for synthetic effort has focused on development of solution processable small molecules to facilitate the fabrication and improve the efficiency of the BHJ solar cells based on small molecules.

Recently, materials based on a diketopyrrolopyrrole (DPP) core have been used as electron donor material for BHJ organic solar cell and demonstrated promising PCE of above 4% in BHJ solar cells. Since DPP core unit has a uniquely planar conjugated bi-cyclic structure that promotes strong π–π stacking providing high hole mobility materials [11b]. It also contains electron carbonyl groups that make DPP core suitable for use as the electron withdrawing unit in low band gap donor–acceptor materials [11,14]. Its derivatives comprised of thiophene moiety can strongly induce the intermolecular π–π interaction and the absorption band shift of longer wavelength absorption by intermolecular charge transfer from thiophene chain to DPP core [15]. Moreover, the DPP based small molecules have been also used as electron acceptors for OPV [16]. Small molecules and polymers derivatives based on DPP have also been used in bilayer OPVs [17].

Here, we report the synthesis of new small molecule containing electron donor diketopyrrolopyrrole (DPP) core and cyanovinylene 4-nitrophenyl (CN) electron acceptor unit DPP–CN as shown in Scheme 1 and used as electron donor for the fabrication of solution processable small molecule based BHJ solar cells along PCBM and modified PCBM, i.e. F and A as electron acceptors. The PCE for the BHJ devices based on DPP–CN:PCBM, DPP–CN:F and DPP–CN:A cast from THF solvent is 1.83%, 2.79% and 2.83%, respectively. The PCE value has been increased to 2.40%, 3.32% and 3.34% for DPP–CN:PCBM, DPP–CN:F and DPP–CN:A blends, respectively cast from mixed solvents. Finally, the device ITO/PEDOT:PSS/DPP–CN:F (DIO/THF cast)/TiO_2/Al device shows a PCE of 3.9%. The improved device performance could be attributed to the electron transporting and hole-blocking capabilities due to the introduced TiO_2 buffer layer.

2. Experimental detail

2.1. Reagents and solvents

Nitrobenzyl cyanide was synthesized from the nitration of benzyl cyanide with concentrated nitric acid and sulfuric acid [17]. It was recrystallized from ethanol, N-N-dimethylformamide (DMF) and tetrahydrofuran (THF) were dried by distillation over CaH_2. The 3,6-bis-(5-bromothiophen-2-yl)-2,5-diethylhexyl-pyrrolo-[3,4-c]-pyrrole-1,4-dione was synthesized according to the literature [18] and dried distillation over CaH_2. All other reagents and solvents were commercially purchased and were used as supplied.

2.2. Synthesis of DPP–CN small molecule

A flask was charged with a solution of 3,6-bis-(5-bromothiophene-2yl)-2,5-diethylhexyl-pyrrolo-[3,4-c]-pyrrole-1,4-dione and cyanovinylene 4-nitrobenzylcyanide (0.1920 g, 1.85 mmol) in ethanol (20 mL). Sodium hydroxide (0.20 g, 5.00 mmol) dissolved in ethanol (10 mL) was added to this reaction. The reaction mixture was stirred for 1 h at room temperature under N_2 and then was concentrated under reduced pressure. The concentrate was cooled in a refrigerator to precipitate in a dark green solid. It was filtered, washed thoroughly with water to afford target small molecule DPP–CN (0.34 g, 74% yield).

We have used diketopyrrolopyrrole DPP–CN small molecule containing 3,6-di(thiophen-2-yl)pyrrolo-[3,4-c]-pyrrole-1,4(2H,5H)-dione (DPP) and cyanovinylene 4-nitrophenyl (CN) units as electron donating and accepting units, respectively as electron donor and PCBM, modified

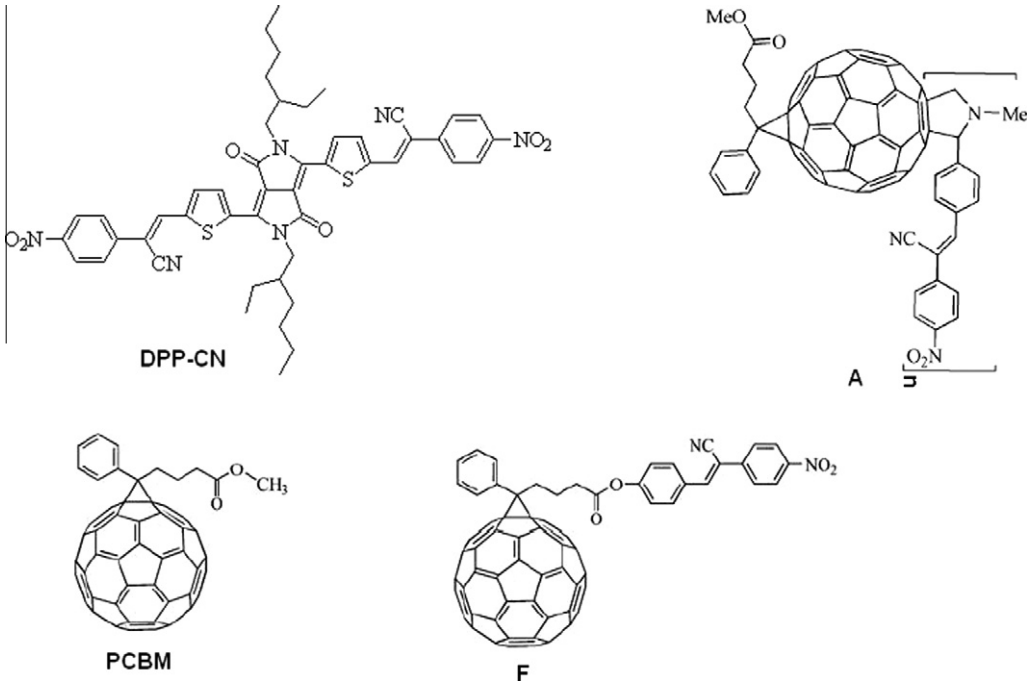

Scheme 1. Chemical structure of DPP–CN, A, PCBM and F.

PCBM i.e. F and A as electron acceptor for the fabrication of BHJ photovoltaic devices. The chemical structure of these materials is shown in Scheme 2. The synthesis of F [19] and A [20] has already been reported. The chemical structures of these materials are shown in Scheme 1.

2.3. Characterization methods

IR spectra were recorded on a Perkin–Elmer 16PC FT–IR spectrometer with KBr pellets. ^{1}H NMR (400 MHz) spectra were obtained using a Bruker spectrometer. UV–vis spectra were recorded on a Beckman DU-640 spectrometer with spectrograde THF. Elemental analyses were carried out with a Carlo Erba model EA1108 analyzer. The XRD patterns of the blend thin films were recorded with an XRD system using CuKα as the radiation source having a wavelength of 1.5405 Å. The atomic force microscopy (AFM) images were recorded with a Digital Instruments nanoscope. The electrochemical properties of DDP–CN were examined using cyclic voltammetry (CV) (EDCA electrochemistry system). The material was coated onto a glassy carbon electrode, which was used as the working electrode, immersed in a 0.1 mol/L Bu_4NPF_6 in acetonitrile solution and used as the supporting electrolyte. Cyclic voltammograms were recorded using Ag/AgCl as the reference electrode at a scan rate of 100 mV/s. A monochromator was used to measure the IPCE spectra of the BHJ photovoltaic devices.

2.4. Computational method

DFT calculations were performed using the Gaussian 09W [21] (Revision-A.02) program suite. The geometry of the dye in air were optimized using density functional theory (DFT) [22] with the hybrid B3LYP [23] density functional and the 6-31G* basis set. The optimized structure was subjected to vibrational analysis, and characterized

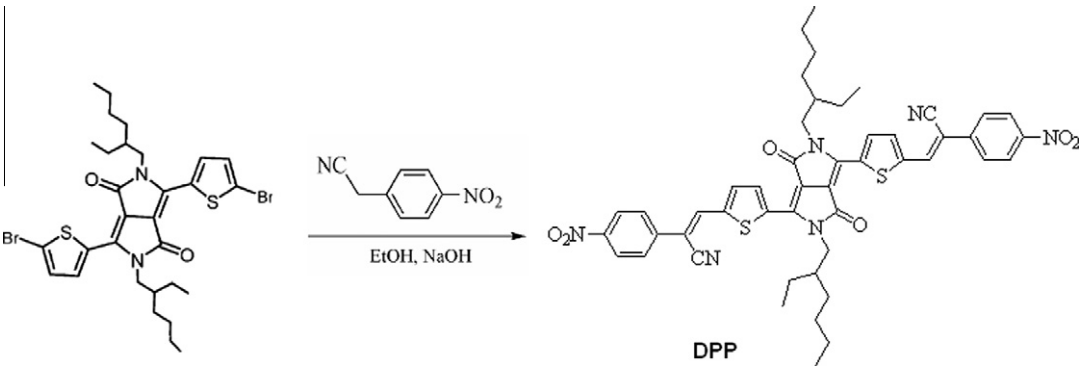

Scheme 2. Synthesis of DPP–CN small molecule.

as a minimum (no imaginary frequencies). The time-dependent DFT (TD–DFT) [24] at the level of B3LYP/6-31G* was further carried out to determine at least 10 vertical excitations to the excited state of the molecule. The computations in THF were performed by applying polarizable continuum model (PCM) using the integral equation formalism variant (IEFPCM) to describe the electrostatic solute–solvent interactions by the creation of solute cavity via a set of overlapping spheres [25]. The absorption spectra were simulated by using the 10 lowest spin-allowed singlet transitions, mixed Lorentzian–Gaussian line shape (0.5) and an average full-width at half maximum (3000 cm^{-1}) for all peaks [26].

2.5. Fabrication and characterization of solar cells devices

BHJ photovoltaic devices were fabricated on an indium tin oxide (ITO) coated glass substrate with ITO coated glass substrate/poly(3,4′-ethylenedioxythiophene:poly(styrenesulfonate) (PEDOT:PSS)/DPP–CN:PCBM or F or A/Al structure. The ITO coated glass substrate was first cleaned with detergent, ultrasonicated in acetone and isopropyl alcohol and subsequently dried overnight in oven. PEDOT:PSS (Baytron) was spin coated from aqueous solution to form a film of thickness about 60 nm. The substrate was dried for 10 min at 80 °C in air and then transferred to a glove box to spin cast the active layer. A solution containing a mixture of DPP–CN: PCBM or F or A (1:1 wt ratio) in THF solvent and mixed solvents (1.5% 1,8-diiodooctane (DIO)/THF) was then spun cast on the top of PEDOT:PSS layer. The film was dried at 50 °C for a 60 min. Then, an aluminum (Al, 80 nm) electrode was deposited by thermal evaporation in a vacuum of about 10^{-6} Torr, using a mask of area 20 mm^2. The effective area of the device is about 20 mm^2. The hole only devices have been fabricated through same method and the top electrode Al was replaced by Au electrode. The electron only devices were fabricated through sandwiching the blend between two Al electrodes.

TiO_2 paste was prepared by mixing of TiO_2 powder (P25 Degussa), 0.2 mL of acetic acid, and 1 mL of de-ionized water. Then 60 mL of ethanol was slowly added while sonicating the mixture for 3 h. Finally Triton X-100 was added to obtain a dispersed colloidal TiO_2 paste. To make the device having structure ITO/PEDOT:PSS/DPP–CN:F/TiO_2/Al, the colloidal nanoparticle TiO_2 paste was spin coated on the active layer at 2500 rpm and then dried, before the deposition of Al electrode.

Current–voltage (*J–V*) characteristics of the devices were measured using a computer controlled Keithley 238 source meter in the dark and under illumination of 100 mW/cm^2 under ambient conditions. A xenon lamp (100 W) was used to give a stimulated irradiance at the surface of device using a 1.5 AM filter.

3. Results and discussion

3.1. Synthesis of DPP–CN

DPP was synthesized as reported in literature [18]. Scheme 2 depicted the outlines of the synthesis of the small molecule DPP–CN. DPP was condensed with cyanovinylene 4-nitrobenzylcyanide to give the targeted DPP–CN small molecule and is soluble in all common organic solvents. The material was characterized by NMR and FTIR spectra.

3.2. Photophysical properties of DPP–CN

The optical properties of DPP–CN were investigated in the solution and thin film cast from the THF solvent. Fig. 1a shows the absorption spectra of DPP–CN in THF solution and thin film. The absorption spectra of DPP–CN show two absorption bands. The peak (~430 nm in both solution and thin film) appeared at short wavelength region is attributed to the π–π* transition in the small molecule chain and the peak (~637 nm and 658 nm for solution and thin film, respectively) appeared in longer wavelength region is attributed to the intramolecular charge transfer between 3,6-di(thiophen-2-yl)pyrrolo-[3,4-c]-pyrrole-1,4(2H,5H)-dione donor unit and cyanovinylene 4-nitrophenyl acceptor unit. It can be seen from Fig. 1a that absorption peak for thin film corresponds to longer wavelength region is red shifted as compared to solution, which may be caused by the existence of some aggregation or π–π stacking of the molecules [27]. The absorption peaks observed in the optical absorption is not sharp, which may be due to the nature of the material i.e. cyanovinylene group attached to the DPP molecule. The absorption onset of DPP–CN small molecule in solution and thin film are at 735 nm and 754 nm, respectively. The optical band gap estimated from the absorption onset of small molecule is 1.64 eV.

The simulated absorption spectra of the DPP–CN in the gas and THF phases are shown in Fig. 1b. The absorption profile predicted for the DPP–CN closely reassembles to that observed for the DPP–CN in THF. The trends observed in the frontier orbital and vertical excitation energies for the two molecules are in agreement with the theoretical predictions. It appears that the central core is a slightly electron-rich owing to the presence of two thiophene moieties and act as a weak donor while the cyanovinylene 4-nitrophenyl unit is the strong acceptor and DPP–CN behaves as D–A small molecule.

3.3. Electrochemical properties of DPP

Fig. 2a shows the cyclic voltammetry (CV) diagram of the DPP–CN small molecule using $TBAPF_6$ as supporting electrolyte in acetonitrile solution with glassy carbon working electrode, a platinum wire electrode and an Ag/AgCl reference electrode. The redox potential of the reference electrode was taken as −4.7 eV relative to the vacuum level. The lowest unoccupied molecular orbital (LUMO) and highest occupied molecular orbital (HOMO) energy level of the DPP–CN were estimated from the onset reduction (E_{red}^{onset}) and oxidation (E_{ox}^{onset}) potential obtained from the cyclic voltammogram, using following expression [28]:

$$\text{HOMO} = -q(E_{ox}^{onset} + 4.7)\ \text{eV}$$
$$\text{LUMO} = -q(E_{red}^{onset} + 4.7)\ \text{eV}$$

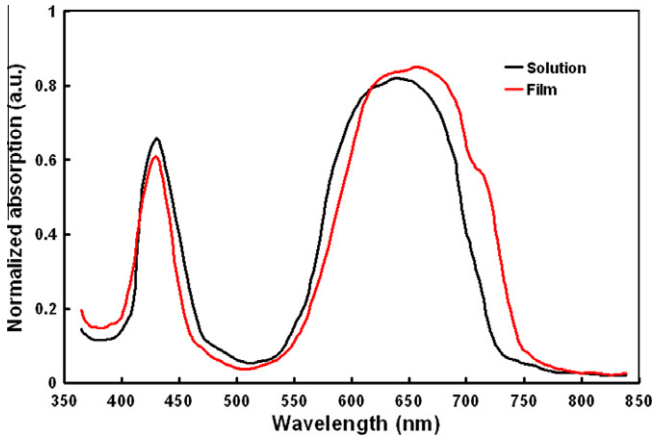

Fig. 1a. Absorption spectra of DPP–CN in THF solution and thin film cast from THF.

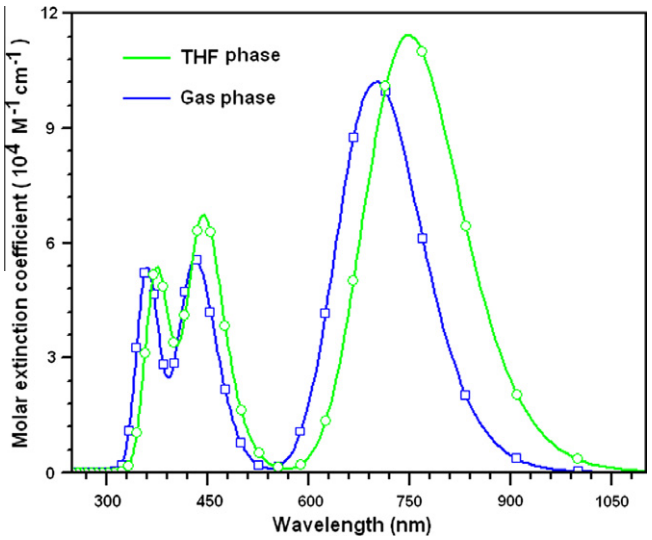

Fig. 1b. Absorption spectra computed for the DPP–CN (fwhm: 3000 cm^{-1}) in gas and THF phase.

The HOMO and LUMO levels of DPP–CN are −5.25 eV and −3.40 eV, respectively, which are very close to the values estimated from DFT calculation. The values HOMO level of PCBM, F and A estimated from cyclic voltammetry are −6.3 eV, 5.9 eV and −5.7 eV, respectively. The HOMO level of DPP–CN is very close to the threshold value HOMO level (−5.2 eV) for a organic semiconductor used as donor in efficient BHJ solar cells [29] and the deeper than that for the most commonly used P3HT donor. In addition, the deeper level of a donor material is desirable for high open circuit voltage (V_{oc}) of BHJ solar cells, because V_{oc} is usually proportional to the difference between the LUMO level of acceptor and HOMO level of donor. The electrochemical band gap is about 1.85 eV estimated from cyclic voltammetry and is slightly higher than the optical band gap, estimated from the UV–visible onset absorption. This is common phenomena in the organic materials due to their higher exciton binding energy [30]. It is generally accepted that an energy difference of 0.3 eV between the LUMO levels of acceptor and donor materials (LUMO–LUMO offset) used in the BHJ is necessary for efficient photo-induced electron transfer from the donor to acceptor [31]. The LUMO levels of PCBM, F and A is −3.95, −3.75 and −3.80 eV, respectively. The LUMO–LUMO offset between DPP and CN and either PCBM or F or A is larger than 0.3 eV and therefore it is expected that excitons can easily dissociated at the donor/acceptor (D/A) interfaces formed between DPP and CN and either PCBM, or F or A. Therefore, DPP–CN can be used as electron donor, with PCBM or F or A as electron acceptor, for BHJ solar cells.

3.4. Electronic properties of DPP from TDDFT calculations

To obtain better rationale for the observed electrochemical properties of the DPP–CN, we have performed TDDFT calculations. The computed vertical excitation and frontier orbital energies, oscillator strengths for electronic excitations and compositions of vertical transitions in

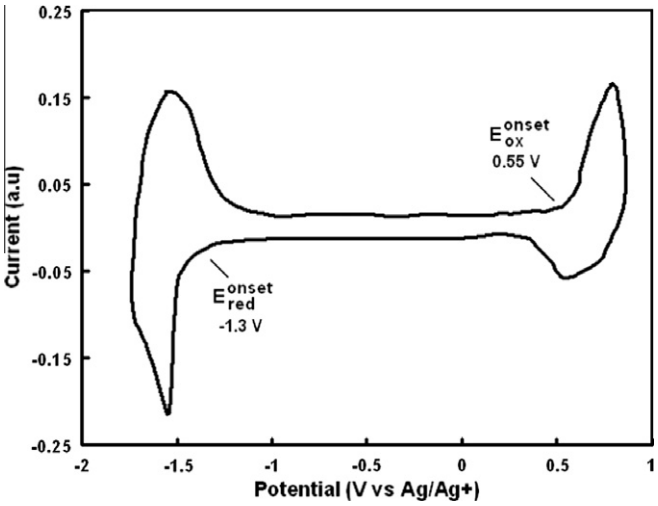

Fig. 2a. Cyclic voltammogram of DPP–CN as scan rate of 100 mV/s.

terms of molecular orbitals are listed in Table 1. The electronic distributions observed for selected molecular orbitals contributing significantly to the prominent electronic excitations in the dye are presented in Fig. 2b. There are three prominent absorptions predicted from the computations for the DPP–CN in gas phase as well as in THF. The lower energy absorption corresponds to the HOMO to LUMO transition while the higher energy transition occurs due to the HOMO to LUMO + 2 and HOMO-2 to LUMO excitations. The HOMO is mainly contributed by the central 3,6-di(thiophen-2-yl)pyrrole-[3,4-c]-pyrrole-1,4(2H,5H)-dione segment while the LUMO is delocalized over the entire molecule. From the electronic distributions in the concerned molecular orbitals the higher energy (low wavelength region) transition occurring in the dye may be described as a π–π^* transition while the HOMO to LUMO + 2 excitation for the higher wavelength transition may cause a charger transfer from the central core to the cyanovinylene 4-nitrophenyl acceptor. The oscillator strengths observed for these transitions in the DPP are in agreement with the extended π-delocalization present in the molecular orbitals. The band gap estimated from these calculations is 1.88 eV and 1.90 eV, in air and THF phase, respectively and is very close to the experimentally observed values.

3.5. Electrical properties of DPP

We have investigated the *J–V* characteristics of DPP–CN using a single layer device having structure ITO/PEDOT:PSS/DPP–CN/Al in dark as shown in Fig. 3. The *J–V* characteristics of the device in the dark show a rectification effect when positive potential is applied to the ITO/PEDOT:PSS electrode with respect to the Al electrode. Since the HOMO level of DPP (−5.25 eV) is very close to the HOMO level of PEDOT:PSS (−5.1 eV), the PEDOT:PSS/DPP interface behaves as Ohmic contact for hole injection from the PEDOT:PSS into the HOMO level of DPP–CN. However, the LUMO level of DPP–CN (−3.40 eV) is very far from the work function of Al (−4.2 eV), the DPP-CN/Al interface behaves as Schottky barrier for the electron injection from the Al into the LUMO level of DPP–CN. Therefore, the rectification observed in the *J–V* characteristics in dark is due to the formation of a Schottky barrier at the Al/DPP-CN interface.

The *J–V* characteristics of the ITO/PEDOT:PSS/DPP–CN/Al device under illumination intensity of 100 mW/cm^2 is also shown in Fig. 3 and the values of J_{sc}, V_{oc} FF and PCE are 0.027 mA/cm^2, 0.71 V, 0.35 and 0.0067%, respectively. In spite of broader absorption band in the visible region and low band gap of DDP, the PCE of the photovoltaic

Table 1
Calculated results for DPP using B3LYP/6-31G(d).

Sample	λ_{max}, nm (eV)	Oscillator strength	Composition	HOMO, eV	LUMO, eV	Band gap, eV	Dipole moment, Debye
595 (air)	700 (1.77)	1.41	HOMO → LUMO (100%)	−5.61	−3.72	1.90	0.366
	459 (2.70)	0.24	HOMO → LUMO + 2 (68%) HOMO-2 → LUMO (29%)				
	427 (2.90)	0.65	HOMO-2 → LUMO (63%) HOMO → LUMO + 2 (30%) HOMO → LUMO + 4 (6%)				
595 (THF)	748 (1.66)	1.58	HOMO → LUMO (99%)	−5.40	−3.52	2.88	0.450
	483 (2.56)	0.13	HOMO → LUMO + 2 (90%) HOMO-2 → LUMO (9%)				
	443 (2.80)	0.88	HOMO-2 → LUMO (84%) HOMO → LUMO + 2 (9%) HOMO → LUMO + 4 (6%)				

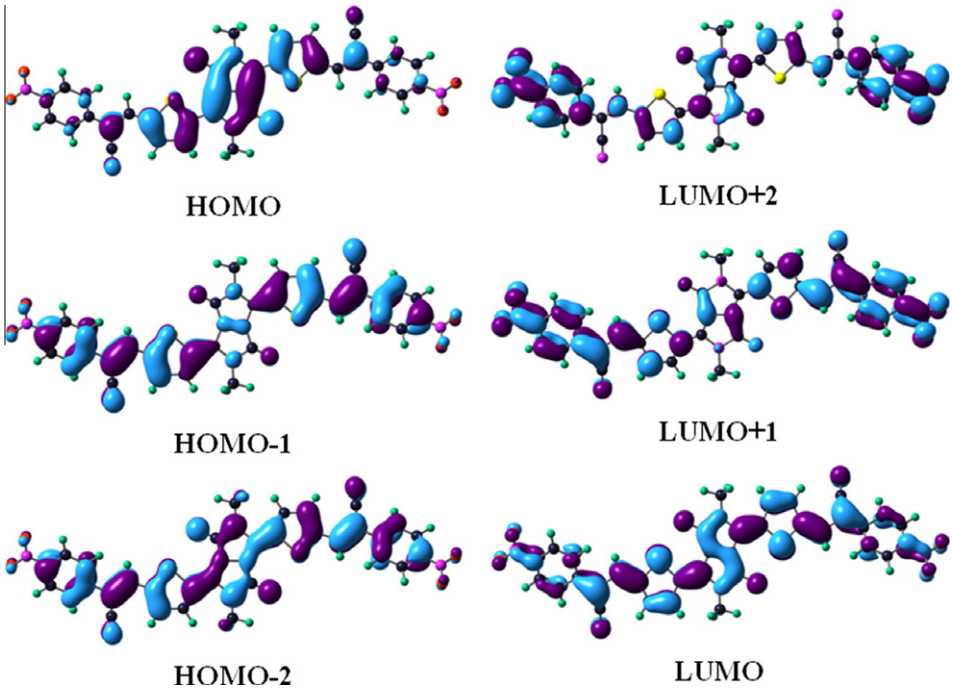

Fig. 2b. Electronic distributions observed for the DPP–CN in selected frontier molecular orbitals contributing significantly to the electronic transitions.

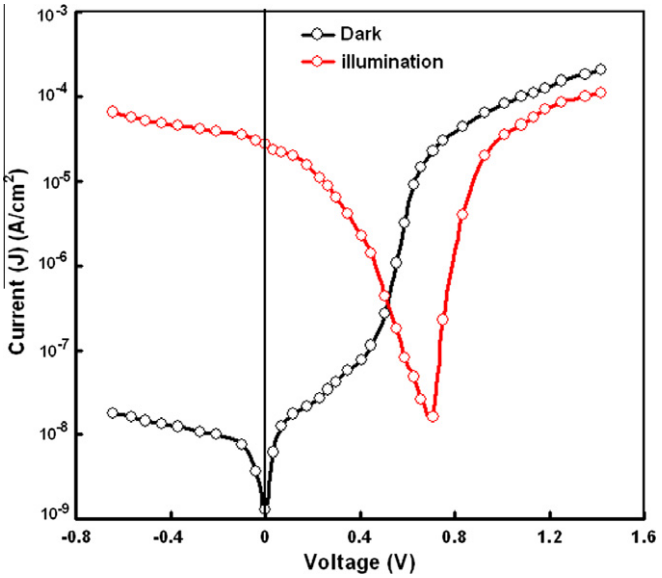

Fig. 3. *J–V* characteristics of ITO/PEDOT:PSS/DPP–CN/Al device in dark and under illumination intensity of 100 mW/cm^2.

device based on DDP–CN is very low. This feature is attributed to the fact that all the excitons generated in the DPP–CN layer, after the absorption of light are not dissociated into the free charge carriers because the short exciton diffusion length (~10–15 nm) as compared to the thickness of DPP–CN layer (~80 nm). Since the built in potential present in at the DPP–CN/Al interface in the ITO/PEDOT:PSS/DPP–CN/Al device is responsible for the exciton dissociation into free charge carrier, only the photogenerated excitons generated near this interface within the distance about 10–15 nm are only contribute to the photocurrent. The excitons generated far away from Al/DPP–CN interface are lost during their diffusion towards this interface and do not contribute to the photocurrent, leading to low FF and PCE.

The hole mobility of the donor materials used in organic PV device is an important factor, which influences the J_{sc} and the PCE of the device. We have fabricated the device

having ITO/PEDOT/PSS/DPP–CN/Au for the estimation of hole mobility in DPP–CN. In this device, both ITO/PEDOT:PSS and Au form the nearly Ohmic contact with DPP–CN layer and the holes are injected from the ITO/PEDOT:PSS electrode into the HOMO of DPP–CN and then collected by the Au electrode, under forward bias i.e. positive potential applied to ITO/PDEOT:PSS with respect to Au. The hole mobility of DPP–CN was measured by space charge limited current (SCLC) method and the hole mobility was estimated to be 3.6×10^{-5} and 8.5×10^{-5} cm^2/V s for the film cast from THF and mixed solvents. The higher hole mobility for the film cast from the mixed solvent is attributed to the improve crystalline nature of DPP–CN film cast from the mixed solvent.

3.6. Optical and XRD properties of BHJ active layers

Fig. 4a shows the UV–visible absorption spectra of DPP–CN:PCBM, DPP–CN:F and DPP–CN:A thin films cast from THF solvent. The absorption peak in the lower wavelength region corresponds to either PCBM or F or A, whereas the absorption band in the longer wavelength region corresponds to DPP–CN. It can be seen from the figure that the absorption intensity for DPP–CN:A is higher in the longer wavelength region and also exhibit broader absorption band in the longer wavelength region as compared to the other blend. This can be attributed to the fact that the A also exhibit a absorption band in the longer wavelength region centered at 610 nm. Therefore we concluded that the absorption band for DPP–CN:A in the longer wavelength region is due to both DPP–CN and A, which indeed increases the absorption intensity of the blend in longer wavelength region. The DPP–CN:F blend shows a broad absorption from 400–720 nm as compared to DPP–CN:PCBM, which is closely matches with the solar spectrum. However, the DPP–CN:A shows a broader absorption band in longer wavelength region with high absorption intensity. Therefore, we expect more photons to be absorbed by the both DPP–CN:F and DPP–CN:A blend as compared to DPP–CN:PCBM.

The optical absorption spectra of the DPP–CN:PCBM, DPP–CN:F and DPP–CN:A blends cast from mixed solvents are shown in Fig. 4b. Upon addition of DIO in the blend solution in THF, the absorption band is slightly red shifted and the intensity is also increased. A higher crystallinity degree of DPP–CN was indicated by red shift in the absorption band in longer wavelength region, which indicates enhanced interchain π–π^* stacking. The blend films cast from the mixed solvents showed higher crystallinity than the cast from THF solvent, which is due to the different vapor pressure and boiling point of the solvents. The improved crystallinity of the blend which is facilitated through self organized chain stacking, can enhance not only the hole transport but also the light harvesting capabilities, thus improving the photocurrent in the PV devices.

Thin film XRD was used to determine the difference in the crystallinity of the pure and blended films cast from THF and mixed solvent. Fig. 5a gives the diffraction patterns of DPP–CN films cast from THF and mixed solvents. As seen in Fig. 5a, the DPP-CN cast from the THF solvent exhibits a peak centered at $2\theta = 6.05°$, which corresponds to an interplanar distance of 1.45 nm. Casting of DPP–CN film from the mixed solvents, leads to higher peak intensity, indicating a higher degree of crystallinity. When blended with different fullerene acceptors (PCBM, F and A) this diffraction peak is not clearly observed as shown in Fig. 5b for DPP–CN:F blend only, suggesting the effectiveness of the fullerene acceptors in interfering with DPP–CN molecular packing. However, when the film of the blends cast from mixed solvent, diffraction peaks again reappear. The diffraction peak for DPP–CN:PCBM is broad and centered at $2\theta = 6.15°$, corresponding to an interplanar distance of 1.43 nm. In comparison, the peaks for the DPP–CN:F and DPP–CN:A are sharp and centered at $2 = 6.10°$, corresponding to an interplanar distance of 1.44 nm. Depending on the type of derivative, most fullerene derivatives such as PCBM do not show any diffraction peaks in the range of 2 values used [32]. The changes in crystallinity of the blended film, therefore, after casting the film from mixed solvent are mainly attributed to an increase in crystallinity domains of the DPP–CN donor material. The increase in the crystallite size also provides further insight onto the effective charge transport and also provides high internal effective field for charge separation, resulting higher value of PCE.

3.7. Photovoltaic properties of BHJ devices

We have carefully examined the PV performance of the devices with different blend ratio and found that the best performance was found for the devices with 1:1 weight ratio of DPP–CN: PCBM or F or A. Fig. 6a shows the *J*–*V* characteristics of the devices with DPP–CN:PCBM or F or A, cast from THF solvent, under illumination intensity of 100 mW/cm^2. Table 2 summaries the various photovoltaic parameters, i.e. short circuit current (J_{sc}), open circuit voltage (V_{oc}), fill factor (FF) and power conversion efficiency (PCE). The J_{sc} of 5.74 mA/cm^2, 6.32 mA/cm^2 and 6.55 mA/cm^2 have been achieved for the devices based on DPP–CN:PCBM, DPP–CN:F and DPP–CN:A blend. Combined with FF (0.38, 0.45 and 0.45 for PCBM, F and A as acceptor respectively) and V_{oc} (0.84 V, 0.98 V and 0.96 V, for PCBM, F and A, respectively), the value of PCE for these devices are 1.83%, 2.79% and 2.83% for DPP–CN:PCBM, DPP–CN:F and DPP–CN:A, respectively. Compared to PCBM based device, the value of PCE for the devices based on F and A is higher which is due to the large increment in the both J_{sc} and V_{oc}. The increase in J_{sc} could be attributed to the more intense absorption of F and A in visible region than that of PCBM as evident from the absorption spectra of the both DPP–CN:F and DPP–CN:A blends. It can be seen that the V_{oc} has increased from 0.84 V for PCBM to 0.98 V and 0.96 V for F and A based devices, respectively. Obviously, the increase in the value of V_{oc} for the PV based on F and A compared to that of PCBM has been attributed to the higher LUMO levels of F or A (−3.80 eV) as compared to PCBM (−3.95 eV), since it is well known that the V_{oc} of the organic BHJ photovoltaic devices is proportional to the difference between the HOMO of the donor and LUMO of the acceptor.

The values of incident photon to current efficiency (IPCE) have been estimated using following expression:

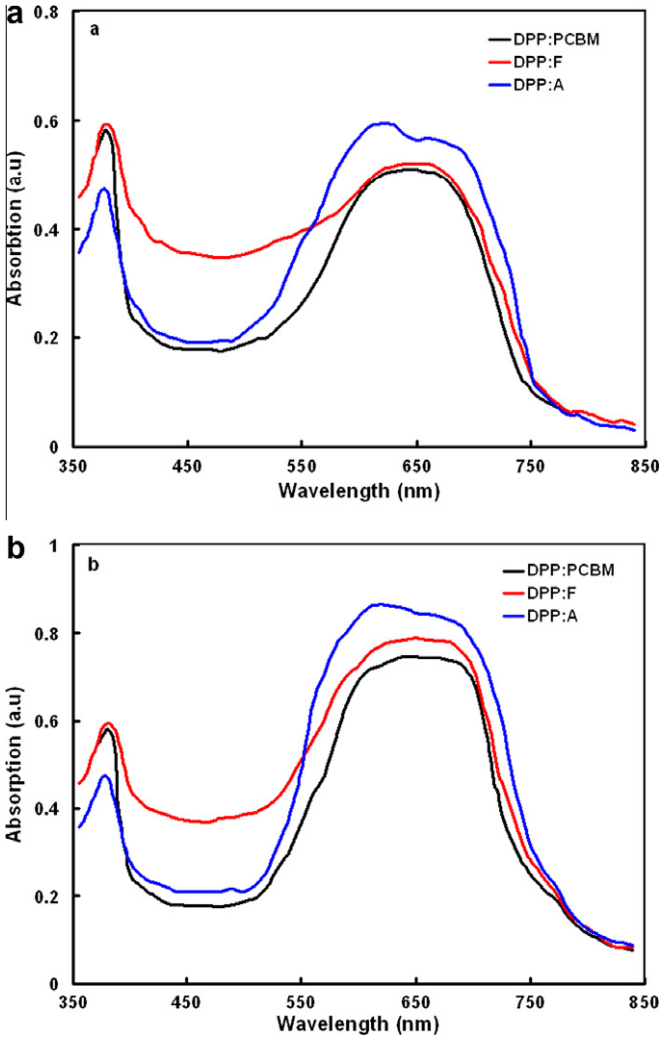

Fig. 4. Absorption spectra of DPP–CN:PCBM, DPP–CN:F and DPP–CN:A thin films cast from (a) THF solvent and (b) mixed DIO/THF solvents.

$$\text{IPCE}\ (\%) = 1240 J_{sc}/P_{in}\ (\text{W/m}^2)\lambda\ (\text{nm})$$

where P_{in} and λ are the illumination intensity and wavelength of the monochromatic light, respectively. The IPCE spectra of the BHJ photovoltaic devices based on DPP–CN:PCBM, DPP–CN:F and DPP–CN:A blends are shown in Fig. 6b. The IPCE spectra of the BHJ photovoltaic devices based on these blends resemble the optical absorption spectra (Fig. 4a) of the respective blends used in the device, indicates that the both components used in the blend contribute to photocurrent generation. The IPCE in the wavelength region 395–560 nm is higher for both the devices based on DPP–CN:F and DPP–CN:A blends than that for DPP–CN:PCBM which can be ascribed to the contribution of absorption of visible light in this region by F and A and contributing to the photocurrent. It can be seen from Fig. 6b that the IPCE spectra is broader in the longer wavelength region for the device based on DPP–CN:A than that for DPP–CN:F. Since the A shows absorption band in longer wavelength region [20], this broader IPCE spectrum for this device may be ascribed to absorption of light by A and contributing to the photocurrent. The IPCE results indicate that the both F and A acceptors are beneficial to the efficient light harvesting of visible light than PCBM and affords higher photocurrent.

The PCE of these devices based on BHJ active layer cast from THF is still low in comparison to that for polymer BHJ devices. The control phase separation in the BHJ active layer play an important role in enhancing the PCE of the BHJ photovoltaic device. A mixed solvents approach has been shown to be effective in several polymer solar cells including P3HT [33] as well as for other low band gap conjugated polymers [34]. This approach has also been successfully applied to other small molecule: fullerene derivatives BHJ devices [35]. The *J–V* characteristics and corresponding IPCE spectra of the devices based on DPP–CN:PCBM, DPP–CN:F and DPP–CN:A cast from mixed (1.5% vol 1,8-diiodooctane DIO/THF) solvents are shown in Fig. 7a and b, respectively. The PV parameters are summarized in Table 2. It can be seen from the table that the in

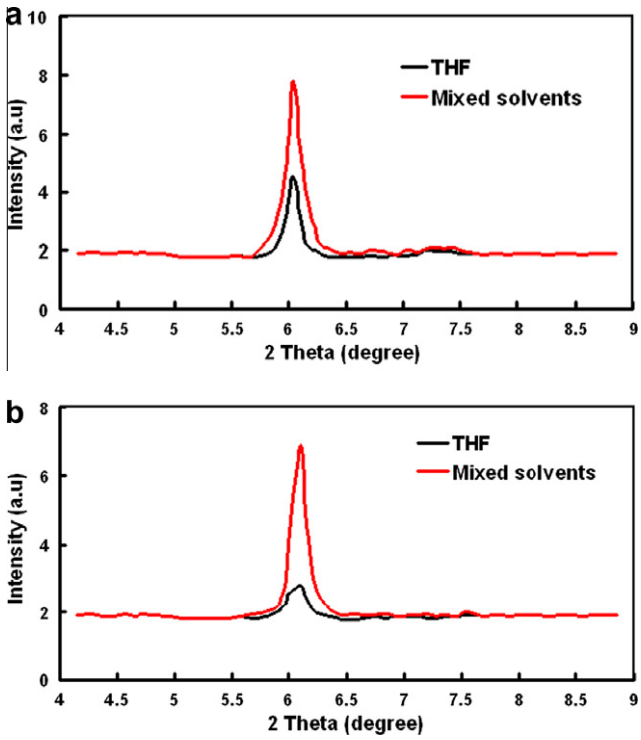

Fig. 5. Diffraction pattern for the (a) DPP–CN and (b) DPP–CN:F films cast from THF solvent and mixed DIO/THF solvents. Similar results have been obtained for other blends also.

all device the PCE has been increased (2.40%, 3.32% and 3.34% for DPP–CN:PCBM, DPP–CN:F and DPP–CN:A, respectively). The improvement in the PCE has been mainly attributed to the mainly to the increase in J_{sc} and FF, while the V_{oc} has been slightly decreased. The IPCE spectra of the devices cast from the mixed solvents (Fig. 7b) also confirm the improvement in the J_{sc}, as indicated by the increase in the IPCE values and broader shape of the IPCE spectra, as compared to the device cast from THF solvent. The redshift in the IPCE spectra of the devices cast from mixed solvent agree with the redshift observed in the absorption spectra of the blends cast from mixed solvent, which is due to the enhancement in the crystallinity of the DPP–CN. The rise in the J_{sc} and IPCE values has been attributed to the increase in the crystallinity and light absorption capability of the BHJ active layer as evidenced from the XRD and absorption spectra of BHJ active layer.

Since, the J_{sc} of the BHJ photovoltaic device is the result of light absorption, exciton dissociation, charge transport and collection by the electrodes. These three mechanisms are also crucial for the overall PCE of the BHJ photovoltaic device. To get information about the effect of DIO additive on the charge transport and collection in the device, we have estimated the hole and electron mobilities in the BHJ active layer, by space charge limited current (SCLC) measurements, with hole/electron only devices. Fig. 8 shows the variation of dark current with applied voltage for hole only device i.e. ITO/PEDOT:PSS/DPP–CN:F/Au, the DPP–CN:F film was cast from THF and mixed solvents. The applied voltage was corrected for built in voltage (V_{bi}). Similar results were also observed for devices based on other blends, i.e. DPP–CN:PCBM and DPP–CN:A. It can be seen from this figure that in low voltage region, the dark current (J_d) is linearly dependent on applied voltage with a slope about unity, which corresponds to Ohmic region. In the higher voltage region, the J_d can also be fitted to be linearly dependent on voltage with slope two, which corresponds to SCLC behavior with trap free limit. The SCLC behavior in this region can be characterized using Mott–Gurney square Law [11]. The hole mobility in the blend can be estimated from following equation:

$$J_{SCLC} = (9/8)\epsilon_r \mu_h (V^2/d^3)$$

where ε_r is the static dielectric constant of the medium and μ_h is the hole mobility, d is the thickness of the active layer and J_{SCLC} is the dark current in SCLC region. The hole mobility of DPP–CN:F cast from THF and mixed solvents evaluated using above Mott–Gurney Law (using $\varepsilon_r = 3.5$) were 1.3×10^{-5} cm^2/V s and 6.8×10^{-4} cm^2/V s, respectively. Same results were also observed for other blends also. As a result, the hole mobility of DPP:F cast from mixed solvents was about more than one order higher than that of cast from THF solvent. From these results we can conclude that casting from mixed solvents improve the hole mobility due to the increased crystallinity of the blend. Therefore, the hole mobility enhancement with the additive is caused by enhanced π–π stacking and chain ordering as supported by UV–visible absorption and X-ray diffraction data. We have also measured the electron mobility in the DPP–CN:F blend using electron only Al/DPP–CN:F/Al device and found that the electron mobility also increases

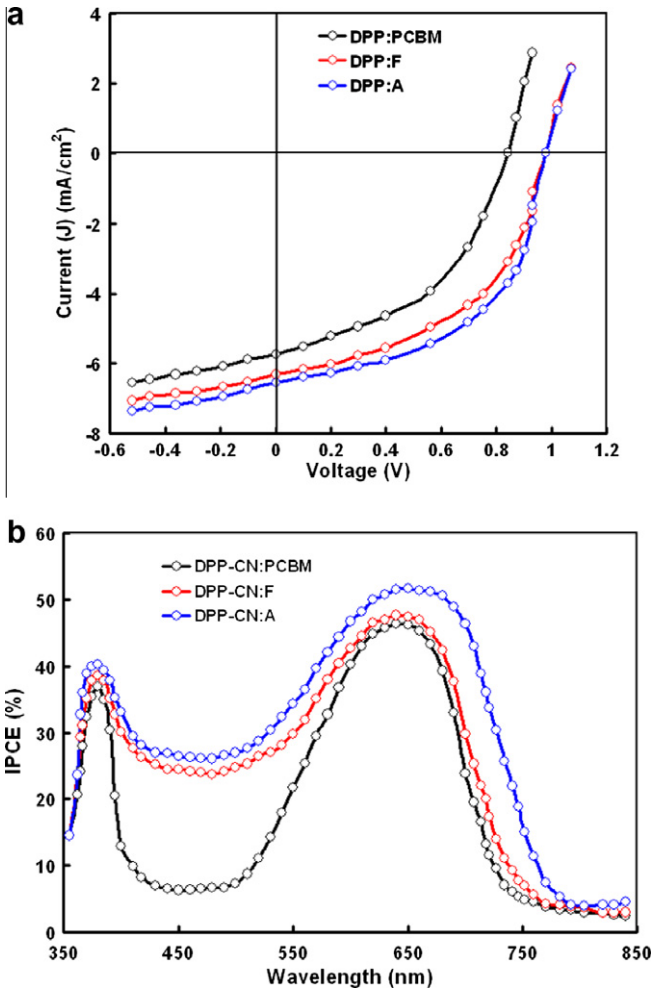

Fig. 6. (a) *J–V* characteristics under illumination (b) IPCE spectra of the BHJ photovoltaic devices based on DPP–CN:PCBM, DPP–CN:F and DPP–CN:A blends cast from THF solvent.

Table 2
Photovoltaic parameters of ITO/PEDOT:PSS/DPP: PCBM or F or A/Al devices cast from different solvents.

Blends	Short circuit current (mA/cm^2)	Open circuit voltage (V_{oc}) (V)	Fill factor (FF)	Power conversion efficiency (PCE) (%)
DPP:PCBM[a]	5.74	0.84	0.38	1.83
DPP:F[a]	6.32	0.98	0.45	2.79
DPP:A[a]	6.55	0.96	0.45	2.83
DPP:PCBM[b]	6.83	0.80	0.44	2.40
DPP:F[b]	7.36	0.94	0.48	3.32
DPP:A[b]	7.7	0.94	0.46	3.34

[a] Cast from THF solvent.
[b] Cast from mixed solvents.

(from 3.4×10^{-4} cm^2/V s to 4.3×10^{-4} cm^2/V s) but the degree of increase in very small in comparison to that for hole mobility. With the hole mobility enhancement and a similar electron mobility, the ratio between these two mobilities reduced, resulting balance charge transport in the device based on blend cast from the mixed solvents as compared to that cast from THF solvent [36].

The surface morphology of the photoactive layer was also investigated using the atomic force microscopy (AFM) and shown in Fig. 9. We have shown only for DPP–CN:F blend film. Similar results have also been observed for other blends. It can be seen from these AFM images that the bigger domains are observed for the blend cast from the THF in comparison to that cast from mixed solvents. Finer domain size attributes to the increase interfacial area of D–A, which leads to an efficient exciton dissociation [37].

To investigate how the film of nanocrystalline TiO_2 NP affects the photovoltaic performance of the device, TiO_2

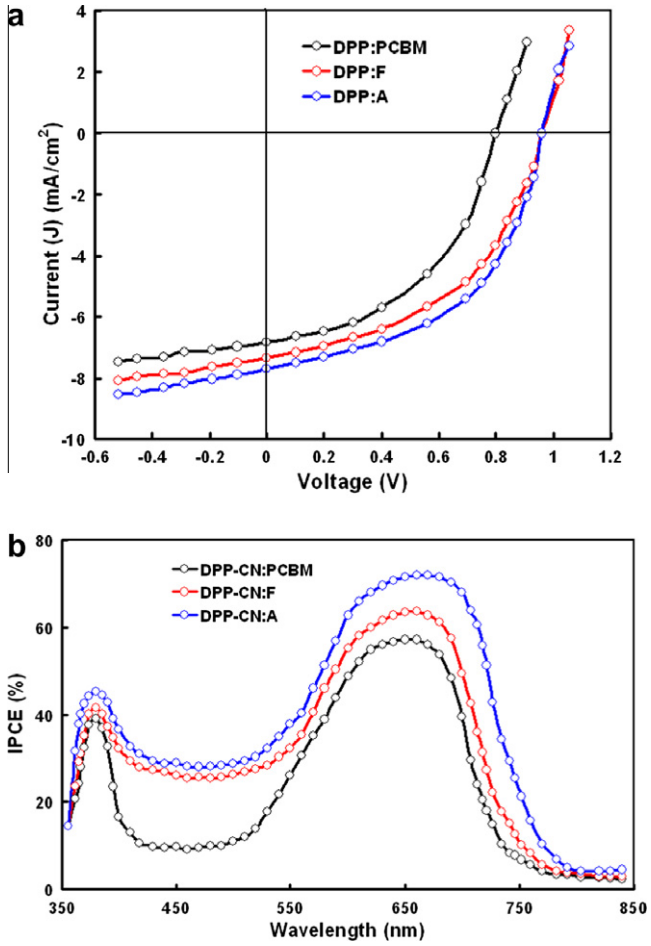

Fig. 7. (a) *J–V* characteristics under illumination (b) IPCE spectra of the BHJ photovoltaic devices based on DPP–CN:PCBM, DPP–CN:F and DPP–CN:A blends cast from DIO/THF mixed solvents.

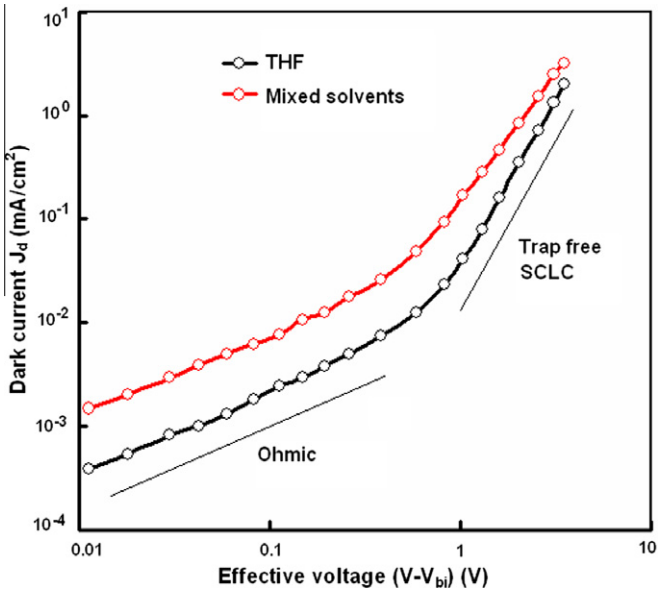

Fig. 8. *J–V* characteristics of hole only devices ITO/PEDOT:PSS/DPP–CN:F/Au, where the DPP–CN:F thin film cast from THF and DIO/THF mixed solvents.

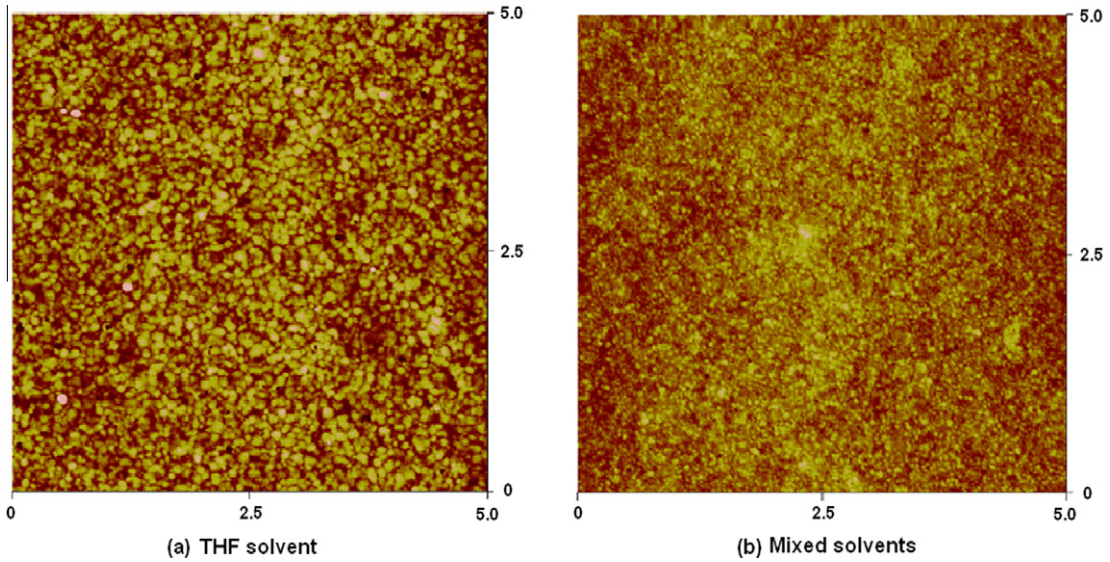

Fig. 9. AFM surface topography of DPP–CN:F thin films cast from (a) THF solvent and (b) Mixed DIO/THFsolvents, the dimensions are 5 μm × 5 μm.

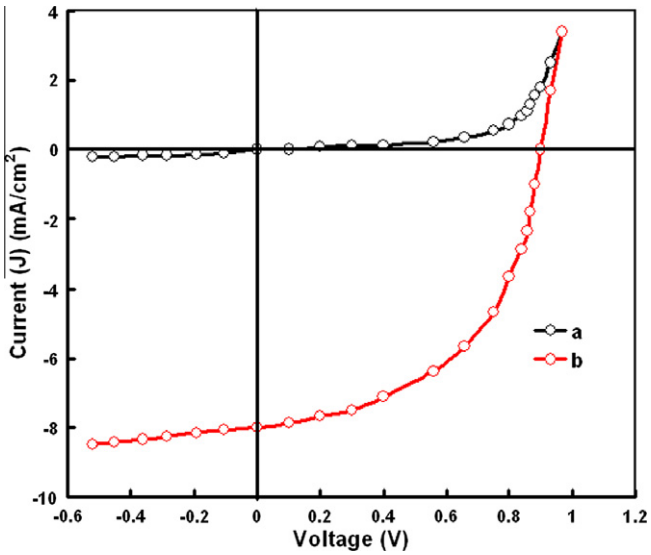

Fig. 10. *J–V* characteristics of ITO/PEDOT:PSS/DPP–CN:A (mixed solvent cast)/TiO_2Al device in dark and under illumination intensity of 100 mW/cm^2.

sol gel was spin coated at 2500 rpm on the top of active layer. The *J–V* characteristics of the ITO/PEDOT:PSS/DPP–CN:A (cast from mixed solvents)/TiO_2/Al device in dark and under illumination are shown in Fig. 10. The device exhibit J_{sc}, V_{oc} and FF 8.0 mA/cm^2, 0.90 V and 0.54, respectively and resulting overall PCE of 3.9%. For the device with TiO_2 buffer layer, the improvement in PCE is mainly drives from both J_{sc} and FF, whereas V_{oc} remain unaffected. It is well known that the V_{oc} can be approximated from the difference between HOMO of donor and LUMO of acceptor used in BHJ active layer. Although the additional TiO_2 layer may help to break the symmetry of the electric field in the device, its conduction band edge (−4.3 eV), which is very close to the Fermi level of Al does not have much contribution to V_{oc}. The improvement in both J_{sc} and FF is expected as the TiO_2 buffer layer functions as electron transport layer (ETL) and hole blocking layer (HBL), inducing a more charge collection and suppresses the charge recombination at active layer–cathode interface. Recently, Lee et al. found that the TiO_x layer in OPV decreases the saturation current density, resulting in reduced minority carrier density [38]. TiO_2 with higher conduction band edge provides high energy barrier for holes, and therefore moderating the charge injection process and leading to higher FF. Besides, used as ETL/HBL layer, the introduction of TiO_2 layer can redistributes the light intensity in the BHJ active layer film, i.e. an optical spacer, which enhances the photon harvesting. It is also observed that with the

incorporation of TiO_2 buffer layer, lowers the series resistance (R_s), while increases the shunt resistance (R_{sh}). The reduction in R_s correlates well with the enhancement in J_{sc} [39]. TiO_2 buffer layer decreases the leakage current of device, since it is used as the protective layer that prevents the charge escaping from the cathode to the active layer. The TiO_2 layer acts as an electron transporting layer and hole-blocking layer in the device.

4. Conclusion

We have investigated the optical, electrochemical and electrical properties of the new DPP–CN small molecules having D–A configuration. It is soluble is common solvent and showed a broad absorption band in longer with a optical band gap of 1.64 eV, which is very close to the electrochemical band gap 1.85 eV. We have fabricated organic BHJ photovoltaic devices based on DPP–CN:PCBM, DPP–CN:F and DPP–CN:A blends cast from THF solvent and mixed (DIO/THF) solvents. The PCE values of these devices based on DPP–CN:PCBM, DPP–CN:F and DPP–CN:A are 1.83%, 2.79% and 2.83%, respectively. The higher value of V_{oc} for the devices based on DPP–CN:F and DPP–CN:A blends with respect to DPP–CN:PCBM has been attributed to the higher LUMO level of F and A with respect to PCBM. The higher values of PCE for the devices based on DPP–CN:F and DPP–CN:A blend ascribed to the higher absorption of both F and A in visible region as compared to PCBM. The PCE of the devices based on DPP–CN:PCBM, DPP–CN:F and DPP–CN:A blends processed from DIO/THF solvent is 2.40%, 3.32% and 3.34%, respectively. The increased value of PCE has resulted from the improved crystalline nature of the blend and morphological change in the film, which in turns enhance the hole mobility. The PCE of the device ITO/PEDOT:PSS/DPP–CN:A (cast from DIO/THF)/TiO_2 has further improved to 3.9%. This improvement has been attributed to the electron transporting and hole-blocking capabilities of TiO_2 buffer layer.

References

[1] (a) S. Gunes, H. Neugebauer, N.S. Sariciftci, Chem. Rev. 107 (2007) 1324–1338;
(b) A.C. Mayer, S.R. Scully, B.E. Hardin, M.W. Rowell, M.D. McGehee, Mater. Today 10 (2007) 28;
(c) R. Po, M. Maggini, N. Camaioni, J. Phys. Chem. C 114 (2010) 695;
(d) B.C. Thompson, J.M. Frechet, Angew. Chem. Int. Ed. 47 (2008) 58–77;
(e) G. Dennler, M.C. Scharber, C.J. Brabec, Adv. Mater. 21 (2009) 1323–1338;
(f) J. Chen, Y. Cao, Acc. Chem. Res. 42 (2009) 1709–1718;
(g) Y.J. Cheng, S.H. Yang, C.S. Hsu, Chem. Rev. 109 (2009) 5868–5923;
(h) V. Shrotriya, Nat. Photon. 3 (2009) 447–449;
(i) F.C. Krebs, Sol. Energy Mater. Sol. Cells 93 (2009) 394–412;
(j) M. Helgesen, R. Sondergaard, F.C. Krebs, J. Mater. Chem. 20 (2010) 36–60;
(k) D. Gendron, M. Leclerc, Energy Environ. Sci. doi:10.1039/c1ee01072g;;
(l) F.C. Krebs, T.D. Nielsen, J. Fyenbo, M. Wadstrom, M.S. Pedersen, Energy Environ. Sci. 3 (2010) 512;
(m) F.C. Krebs, T. Tromholt, M. Jorgensen, Nanoscale 2 (2010) 873.

[2] (a) N.S. Sariciftci, L. Smilowitz, A.J. Heeger, F. Wudl, Science 258 (1992) 1474–1478;
(b) G. Yu, J. Gao, J.C. Hummelen, F. Wudl, A.J. Heeger, Science 270 (1995) 1789–1791.

[3] G. Dennler, M.C. Scharber, T. Ameri, P. Denk, K. Forberich, C. Waldauf, C.J. Brabec, Adv. Mater. 20 (2008) 579.

[4] (a) L. Hou, J. Hou, S. Zhang, H.Y. Chen, Y. Yang, Angew. Chem. Int. Ed. 49 (2010) 1500;
(b) J. Hou, H.Y. Chen, S. Zhang, G. Li, Y. Yang, J. Am. Chem. Soc. 130 (2008) 16144;
(c) Y. Zou, A. Naiari, P. Berrouard, S. Beaupre, B.R. Arich, Y. Tao, M. Leclerc, J. Am. Chem. Soc. 132 (2010) 5330;
(d) R. Qin, W. Li, C. Li, D. Du, C. Veit, H.F. Schleiermacher, M. Andersson, Z. Bo, Z. Liu, O. Inganas, U. Wuerfel, F. Zhang, J. Am. Chem. Soc. 131 (2009) 14612;
(e) H.Y. Chen, J. Hou, S. Zhang, Y. Liang, G. Yang, L. Yu, Y. Wu, G. Li, Nat. Photon. 3 (2009) 649;
(f) S.H. Park, A. Roy, S.J. Beaupre, S. Cho, N. Coates, J.S. Moon, D. Moses, M. Leclerc, K. Lee, A.J. Heeger, Nat. Photon. 3 (2009) 297;
(g) Y. Linag, Z. Xu, J. Xiu, S.T. Tsai, Y. Wu, G. Li, C. Ray, L. Yu, Adv. Mater. 22 (2010) E135;
(h) S.C. Price, A. C. Stuart, L. Yang, H. Zhou, W. You, J. Am. Chem. Soc. doi:10.1021/ja1112595;;
(i) T.Y. Chu, J. Lu, S.Beaupre, Y. Zhang, J.R. Pouliot, S. Wakim, J. Zhou, M. Leclerc, Z. Li, J. Ding, Y. Tao, J. Am. Chem. Soc, doi:10.1021/ja200314;;
(j) C.V. Hoven, X.D. Dang, R.C. Coffin, J. Peet, T.Q. Nguyen, G.C. Bazan, Adv. Mater. 22 (2010) E63–E66;
(k) J. Peet, J.Y. Kim, N.E. Coates, W.L. Ma, D. Moses, A.J. Heeger, G.C. Bazan, Nat. Mater. 6 (2007) 497–500.

[5] (a) www.solarmer.com; (b) www.konarka.com.

[6] (a) F.C. Krebs, R.B. Nyberg, M. Jorgensen, Chem. Mater. 16 (2004) 1313–1318;
(b) K.T. Nielsen, K. Bechgaard, F.C. Krebs, Macromolecules 38 (2005) 658–659.

[7] C. Goh, R.J. Kline, M.D. McGehee, E.N. Kadnikova, J.M.J. Frecher, Appl. Phys. Lett. 86 (2005) 1221101–1221103.

[8] (a) M.T. Lloyd, J.E. Anthony, G.G. Malliaras, Mater. Today 10 (2007) 34;
(b) J. Roncali, Acc. Chem. Res. 42 (2009) 1719;
(c) B. Walker, C. Kim, T.Q. Nguyen, Chem. Mater. doi:10.1021/cm102189g.

[9] (a) C.Q. Ma, M. Fonrodona, M.C. Schikora, M.M. Wienk, R.A. Janssen, P. Bauerle, Adv. Funct. Mater. 18 (2008) 3323;
(b) W.W.H. Ma, C.Q. Wong, W. Pisula, C. Yan, X.L. Feng, D.J. Jones, K. Mullen, R.A.J. Janssen, P. Bauerle, A.B. Holmes, Chem. Mater. 22 (2010) 457;
(c) S. Roquet, A. Cravino, P. Leriche, O. Aleveque, P. Frere, J. Roncali, J. Am. Chem. Soc. 128 (2006) 3459–3466;
(d) W.W. Li, C. Du, F.H. Li, Y. Zhou, M. Fahiman, Z.S. Bo, F.L. Zhang, Chem. Mater. 21 (2009) 5327;
(e) J. Zhang, Y. Yang, C. He, Y.J. He, G.J. Zhao, Y.F. Li, Macromolecules 42 (2009) 7619;
(f) F. Lincker, N. Delbosc, S. Bailly, R. De Bettignies, M. Billon, A. Pron, R. Demadrille, Adv. Funct. Mater. 18 (2008) 3444;
(g) W. Zhang, S.C. Tse, J. Lu, Y. Tao, M.S. Wong, J. Mater. Chem. 20 (2010) 2182;
(h) X. Zhao, C. Piliego, B. Kim, D.A. Poulsen, B. Ma, D.A. Unruh, J.M.J. Frechet, Chem. Mater. 22 (2010) 2325;
(i) G. Wei, S. Wang, K. Renshaw, M.E. Thompson, S.R. Forrest, ACS Nano 4 (2010) 1927;
(j) T. Rousseau, A. Cravino, E. Ripaud, P. Leriche, S. Rihn, A. Nicola, R. Ziessel, J. Ronacali, Chem. Commun. 46 (2010) 5082.

[10] (a) H. Burckstummer, N.M. Kronenber, M. Gsanger, M. Stolte, K. Meerholz, F. Wurthner, J. Mater. Chem. 20 (2010) 240;
(b) Z.J. Ning, H. Tian, Chem. Commun (2009) 5483;
(c) J.A. Mikroyannidis, M.M. Stylianakis, P. Balraju, P. suresh, G.D. Sharma, ACS Appl. Mater. Interfaces 1 (2009) 1711;
(d) Y. Yang, J. Zhang, Y. Zhou, G. Zhan, C. He, Y. Li, M. Andersson, O. Inganas, F. Zhang, J. Phys. Chem. C 114 (2010) 3701;
(e) H.J. Fan, H.X. Shang, Y.F. Li, X.W. Zhan, Appl. Phys. Lett. 97 (2010) 133302;
(f) H. Shang, H. Fan, Y. Liu, W. Hu, Y. Li, X. Zhan, Adv. Mater. doi:10.1002/adma.201004445;
(g) Z. Li, Q. Dong, Y. Li, B. Xu, M. Deng, J. Pei, J. Zhang, F. Chen, S. Wen, Y. Gao, W. Tian, J. Mater. Chem. doi:10.1039/c0jm02510k;
(h) J. Zhang, G. Wu, C. He, D. Deng, Y. Li, J. Mater. Chem. doi:10.1039/C0jm03425h;
(i) Y. Li, Q. Gao, Z. Li, J. Pei, W. Tian, Energy Environ. Sci. doi:10.1039/c003946b;
(j) J.A. Mikroyannidis, D.V. Tsagkournos, S.S. Sharma, Y.K. Vijay, G.D. Sharma, J. Mater. Chem. 21 (2011) 4679.

[11] (a) B. Walker, A.B. Tamayo, X. Dung, P. Zalar, J.H. Seo, A. Garcia, M. Tantiwiwat, T.Q. Nguyen, Adv. Funct. Mater. 19 (2009) 3063;
(b) A.B. Tamayo, B. Walker, T.Q. Nguyen, J. Phys. Chem. C 112 (2008) 11545–11551;

(c) A.B. Tamayo, X.D. Dang, B. Walker, J. Seo, T. Kent, T.Q. Nguyen, Appl. Phys. Lett. 94 (2009) 103301;
(d) A. Tamayo, T. Kent, M. Tantitiwat, M.A. Dante, J. Rogers, T.Q. Nguyen, Energy Environ. Sci. 2 (2009) 1180–1186;
(e) Y. Liu, X. Wan, F. Wang, J. Zhou, G. Long, J. Tian, J. You, Y. Yang, Y. Chen, Adv. Energy Mater. doi:10.1002/aenm.20110230.

[12] (a) H. Shang, H. Fan, Q. Shi, S. Li, Y. Li, X. Zhan, Sol. Energy Mater. Sol. Cells 94 (2010) 457–464;
(b) L.I. Xue, J.T. He, X. Gu, Z.F. Yang, B. Xu, W.J. Tian, J. Phys. Chem. C 113 (2009) 12911–12917;
(c) Z.F. Li, Q.F. Dong, Y.W. Li, B. Xu, M. Deng, J.N. Pei, J.B. Zhang, F.P. Chen, S.P. Wen, Y.J. Gao, W.J. Tian, J. Mater. Chem. 21 (2011) 2159–2168.

[13] Q. Peng, K. Park, T. Lin, M. Durstock, L. Dai, J. Phys. Chem. B 112 (2008) 2801–2808.

[14] L. Huo, J. Hou, H.Y. Chen, S. Zhang, Y. Jiang, T.L. Chen, Y. Yang, Macromolecules 42 (2009) 6564–6571.

[15] A.B. Tamayo, M. Tantiwiwat, B. Walker, T.Q. Nyguen, J. Phys. Chem. C 112 (2008) 15543–15552.

[16] (a) P. Sonar, G.M. Ng, T.T. Lin, A. Dodabalapur, Z.K. Chen, J. Mater. Chem. 20 (2010) 3626;
(b) B.P. Karsten, J.C. Bijleveld, R.A.J. Janseen, Macromol. Rapid Commun. 31 (2010) 1554.

[17] (a) E. Zhou, S. Yamakawa, K. Tamjima, C. Yang, K. Hashimoto, Chem. Mater. 21 (2009) 4055;
(b) M.M. Wienk, M. Turblez, J. Gilot, R.A.J. Janssen, Adv. Mater. 20 (2008) 2556;
(c) L. Burgi, M. Turbiez, R. Pfeiffer, F. Bienewald, H.J. Kirner, C. Winnewissner, Adv. Mater. 20 (2008) 2217;
(d) W. Kylberg, P. Sonar, J. Heier, J.N. Tisserant, C. Muller, F. Nuesch, Z.K. Chen, A. Dodabalapur, S. Yoon, R. Hany, Energy Environ. Sci. doi:10.1039/c1ee01544c

[18] G.R. Robertson, Organic Syntheses, Wiley, New York, 1941.

[19] E.J. Zhou, S.P. Yamakawa, K. Tajima, C.H. Yang, K. Hashimoto, Chem. Mater. 21 (2009) 4055.

[20] J.A. Mikroyannidis, A.N. Kabanakis, S.S. Sharma, G.D. Sharma, Adv. Funct. Mater. 21 (2011) 746–755.

[21] J.A. Mikroyannidis, D.V. Tsagkournos, S.S. Sharma, G.D. Sharma, J. Phys. Chem. 115 (2011) 7806–7816.

[22] M.J. Frisch, G.W. Trucks, H.B. Schlegel, G.E. Scuseria, M.A. Robb, J.R. Cheeseman, G. Scalmani, V. Barone, B. Mennucci, G.A. Petersson, H. Nakatsuji, M. Caricato, X. Li, H.P. Hratchian, A.F. Izmaylov, J. Bloino, G. Zheng, J.L. Sonnenberg, M. Hada, M. Ehara, K. Toyota, R. Fukuda, J. Hasegawa, M. Ishida, T. Nakajima, Y. Honda, O. Kitao, H. Nakai, T. Vreven, J. A. Montgomery, Jr., J.E. Peralta, F. Ogliaro, M. Bearpark, J.J. Heyd, E. Brothers, K.N. Kudin, V.N. Staroverov, R. Kobayashi, J. Normand, K. Raghavachari, A. Rendell, J.C. Burant, S.S. Iyengar, J. Tomasi, M. Cossi, N. Rega, N.J. Millam, M. Klene, J.E. Knox, J.B. Cross, V. Bakken, C. Adamo, J. Jaramillo, R. Gomperts, R.E. Stratmann, O. Yazyev, A.J. Austin, R. Cammi, C. Pomelli, J.W. Ochterski, R.L. Martin, K. Morokuma, V.G. Zakrzewski, G.A. Voth, P. Salvador, J.J. Dannenberg, S. Dapprich, A.D. Daniels, Ö. Farkas, J.B. Foresman, J.V. Ortiz, J. Cioslowski, D.J. Fox, Gaussian 09, Revision A.02, Gaussian, Inc., Wallingford CT, 2009.

[23] (a) W. Kohn, L. Sham, J. Phys. Rev. 140 (1965) A1133–A1138;
(b) R.G. Parr, W. Yang, Density-functional theory of atoms molecules, Oxford University Press, Oxford, 1989.

[24] (a) A.D. Becke, J. Chem. Phys. 98 (1993) 5648–5652;
(b) C. Lee, W. Yang, R.G. Parr, Phys. Rev. B 37 (1988) 785–789.

[25] F. Furche, R. Ahlrichs, J. Chem. Phys. 117 (2002) 7433–7447.

[26] J. Tomasi, B. Mennucci, R. Cammi, Chem. Rev. 105 (2005) 2999–3093.

[27] (a) S.I. Gorelsky, S. Wizard program, http://www.sg-chem.net/, University of Ottawa, Ottawa, Canada, 2010;
(b) S.I. Gorelsky, A.B.P. Lever, J. Organomet. Chem. 635 (2001) 187–196.

[28] (a) Z.F. Li, J.N. Pri, Y.W. Li, B. Xu, M. Deng, Z, Y. Liu, H. Li, H.G. Lu, Q. Li, W.J. Tian, J. Phys. Chem. C (2010) 114 18270–18278;
(b) S. Cho, J.H. Seo, S.H. Kim, S. Song, Y. Jin, K. Lee, H. Suh, A.J. Heeger, Appl. Phys. Lett. 93 (2008) 263301.

[29] (a) J.H. Hou, Z.A. Tan, Y. Yan, Y.J. He, C.H. Yang, Y.F. Li, J. Am. Chem. Soc. 128 (2006) 4911;
(b) Q.J. Sun, H.Q. Wang, C.H. Yang, Y.F. Li, J. Mater. Chem. 13 (2003) 800.

[30] (a) B.C. Thompson, Y.G. Kim, J.R. Reynolds, Macromolecules 38 (2005) 5339;
(b) D.M. de Leeuw, M.M.J. Simenon, A.R. Brown, R.E.F. Einerhand, Synth. Met. 87 (1997) 53.

[31] Y. Zhu, R.D. Champion, S.A. Jeneka, Macromolecules 39 (2006) 871.

[32] A.P. Zoombelt, M. Fonrodona, M.G.R. Turblez, M.M. Wienk, R.A.J. Janssen, J. Mater. Chem. 19 (2009) 5336.

[33] M. Chikamatsu, S. Nagamatsu, Y. Yoshida, K. Saito, K. Yase, Appl. Phys. Lett. 87 (2005) 2035041–2035043.

[34] Y. Yao, J.H. Hou, Z. Hu, G. Li, Y. Yang, Adv. Funct. Mater. 18 (2008) 1783–1789.

[35] (a) J. Peet, M.I. Senatore, A.J. Hegger, G.C. Bazan, Adv. Funct. Mater. 21 (2009) 1521;
(b) J.S. Moon, C.J. Takacs, S. Cho, R.C. Coffin, H. Kim, G.C. Bazan, A.J. Heeger, Nano. Lett. 10 (2010) 4005–4008;
(c) J.H. Kim, J.H. Park, J.H. Lee, J.S. Kim, M. Sim, C. Shim, K. Cho, J. Mater. Chem. 20 (2010) 7398–7405.

[36] (a) H. Fan, H. Shang, Y. Li, X. Zhan, Appl. Phys. Lett. 97 (2010) 133302;
(b) B. Walker, C. Kim, T.Q. Nguyen, Chem. Mater. 23 (2010) 470–482.

[37] (a) P.W.M. Blom, M.J.M. de Jong, M.C. van Munster, Phys. Rev. B 53 (1997) R656–R659;
(b) P.W.M. Blom, V.D. Mihailetchi, L.J.A. Koster, D.E. Markov, Ad. Mater. 19 (2007) 1551–1566.

[38] J.H. Lee, S. Cho, A. Roy, H.T. Jung, A.J. Heeger, Appl. Phys. Lett. 96 (2010) 163303.

[39] (a) M.S. Kim, B.G. Kim, J. Kim, ACS Appl. Mater. Interfaces 1 (2009) 1264–1269;
(b) J.D. Servaties, S. Yenagen, T.J. Marks, M.A. Ratner, Adv. Funct. Mater. 20 (2010) 97–104.